A PHOTO-NEUTRON SOURCE FOR TIME-OF-FLIGHT MEASUREMENTS AT THE RADIATION SOURCE ELBE

Eberhard Altstadt, Carsten Beckert, Hartwig Freiesleben[1], Vladimir Galindo, Eckart Grosse[2], Arnd R. Junghans[2], Joakim Klug[2], Bärbel Naumann[1], Steffen Schneider, Rainer Schlenk, Andreas Wagner[2] and Frank-Peter Weiss

1. Introduction

The radiation source ELBE (Electron Linear accelerator with high Brilliance and low Emittance) at Forschungszentrum Dresden-Rossendorf produces an electron beam that allows to generate sub-ns neutron pulses by stopping the electrons in a heavy radiator and producing neutrons by bremsstrahlung photons through (γ,n)-reactions. In order to enable measurements of energy resolved neutron cross sections like (n,γ), (n,n′γ), (n,p), (n,α), and (n,f) at a time-of-flight arrangement with a short flight path of only a few meters it is necessary to keep the volume of the radiator for neutron production as small as possible to avoid multiple scattering of the emerging neutrons, which would broaden the neutron pulses. The power deposition of the electron beam in the small radiator volume of 1 cm^3 reaches up to 25 kW. This is such a high power density that any solid high Z number material would melt. Therefore, the neutron radiator consists of liquid lead circulated by an electromagnetic pump. From the thermal and mechanical point of view, molybdenum turned out to be the most suited target wall material in the region where the electrons impinge on the radiator.

The measurement of neutron induced reaction cross sections for fusion and fission reactors, and for accelerator driven systems aiming at the transmutation of nuclear waste is the main task to be pursued at the photo-neutron source. The transmutation of long-lived radioactive nuclides is currently discussed [1] to reduce the necessary safe isolation time of radioactive waste in geological disposals and is among others subject of the Integrated EU-project EUROTRANS [2]. A topical overview on the state of the art in nuclear cross sections and on the relevant deficits is given in [3]. Requests are also made for neutron cross sections which are placed in the relevant energy range at ELBE between 50 keV and 10 MeV. Furthermore, experiments can be performed at ELBE which address problems of nuclear astrophysics.

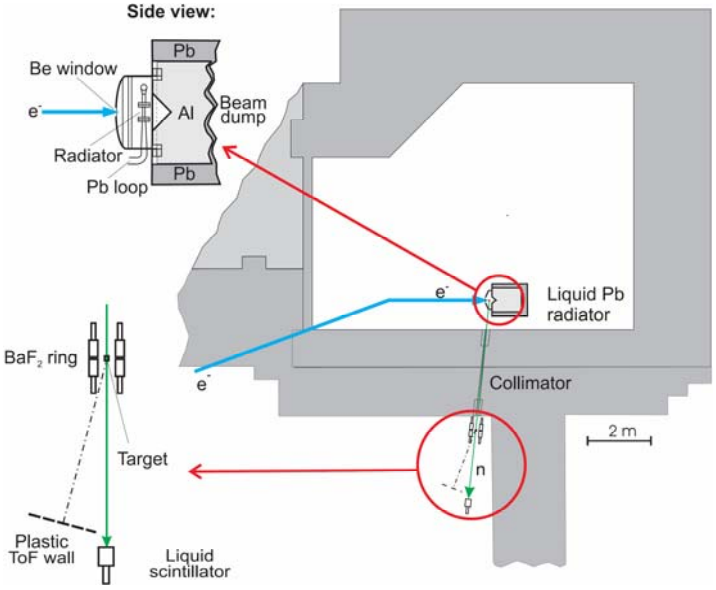

Fig. 1: Floor plan of the n-ToF set-up in the neutron cave. Inserts show a side view of the liquid lead neutron radiator and the detector arrangement in the measuring hall

A sketch of the whole time-of-flight facility (ELBE n-TOF) is shown in Fig. 1. After passing through two thin (200 μm) beryllium windows, the electron beam of ELBE is directed onto the

[1] Technische Universität Dresden, Institute for Nuclear and Particle Physics
[2] Forschungszentrum Dresden-Rossendorf, Institute of Radiation Physics

neutron radiator inside a vacuum chamber where bremsstrahlung photons are produced, generating photo-neutrons by (γ,n)-reactions. In this way, the electron pulse structure is transformed into a similar pulse structure of the neutrons needed for time-of-flight experiments. The neutrons, which are emitted at an angle of about 90°, are decoupled to the measuring position through a collimator in the shielding concrete wall of 2.4 m thickness. A flight path of about 3.9 m is sufficient to separate the neutron pulses from the bremsstrahlung flashes and secondary electrons. A beam dump is located in the primary beam direction behind the neutron radiator and forms part of the vacuum housing. Particle transport calculations predict a neutron source strength in the range of $7.9 \cdot 10^{12}$ n/s to $2.7 \cdot 10^{13}$ n/s for electron energies between E_{e^-} = 20 and 40 MeV. At the measuring place 3.9 m away from the radiator, an average neutron flux of about $1.5 \cdot 10^{7}$ n/(cm² s) will be obtained. The short beam pulses allow for a neutron energy resolution of better than 1 % for neutron energies between E_n = 50 keV and 5 MeV. The usable energies range up to about 10 MeV.

2. Beam parameters of the radiation source ELBE

The ELBE radiation source is centered around a superconducting electron LINAC which produces quasi-continuous electron beams, whose energy can be varied up to E_{e^-} = 40 MeV. Beam intensities of up to I_{e^-} = 1 mA can be delivered with a wide variability in the electron pulse structure. The maximum frequency is f_{e^-} = 260 MHz. This frequency can be lowered by factors of 2^n. The pulse length is less than 10 ps. Picosecond electron pulses will also be used to generate sub-ns neutron pulses. The small emittance of the electron beam at the radiator ($\varepsilon_{RMS} \approx 10\pi$ mm·mrad) permits the irradiation of very small radiator volumes. A new superconducting radio frequency photo electron injector (SRF gun) is being developed, allowing for an unreduced beam current of I_{e^-} =1 mA at a repetition rate of f_{e^-} = 0.5 MHz [4]. With this new photo gun, the measurable neutron energy ranges from E_n = 50 keV to 10 MeV.

As can be seen in Table 1, the ELBE n-TOF set-up has a very competitive luminosity in the accessible energy range compared with all existing high-resolution neutron beams. The proton-accelerator based sources at Los Alamos and the planned Oak Ridge Neutron Spallation Source lose a significant part of their intensity advantage over ELBE when they increase their flight path in order to reach an energy resolution better than 1 %, as expected for ELBE.

Table 1: Parameters of operational and planned neutron time-of-flight facilities

Facility	**CERN n_TOF**		**LANL NSC**	**ORNL SNS**	**FZK VdG**	**ORNL ORELA**	**IRMM GELINA**	**ELBE**	**ELBE with SRF**
Pulse charge [nC]	≈ 10^3		$4 \cdot 10^3$	$3 \cdot 10^4$	0.01	≈ 100	≈ 100	0.08	2
Power [kW]	10		60	1000	0.4	8	7	5	40
Pulse rate [s^{-1}]	0.4		20	60	$2.5 \cdot 10^5$	500	800	$1.6 \cdot 10^6$	$5 \cdot 10^5$
Flight path [m]	183	≈20 in Phase-2	60	84	0.8	40	20	3.9	3.9
n pulse length [ns]	> 7		125	100-700	≈ 1	> 4	> 1	< 0.4	< 0.4
E_{min} [eV]	0.1		1	0.1	10^3	10	10	$2 \cdot 10^5$	$5 \cdot 10^4$
E_{max} [eV]	$3 \cdot 10^8$		≈ 10^8	≈ 10^8	$2 \cdot 10^5$	$5 \cdot 10^6$	$4 \cdot 10^6$	10^7	10^7
Resol. at 1 MeV [%]	0.5	5 in Phase-2	≈ 10	> 10	≈ 10	< 1	< 2	≈ 1	≈ 1
n flux density [s^{-1} cm^{-2} E-decade^{-1}]	10^5	≈ 10^7 inPhase-2	≈ 10^6	10^6 -10^7	≈ 10^4	10^4	$4 \cdot 10^4$	$4 \cdot 10^5$	$3 \cdot 10^6$

3. Design of the main components

The construction of the pulsed photo-neutron source was preceded by detailed simulations, which did not only include the generation of neutrons in the radiator, their transport through the collimator, the background radiation, activation, and shielding but also the thermal stress

and strain in the components hit by the electron beam. A detailed description of these calculations can be found in [5, 6]. A technical concept for the liquid Pb loop was elaborated. A prototype of this loop was constructed and operated in order to study the materials compatibility of the liquid Pb with different wall materials and to test the control regime of the heat exchanger.

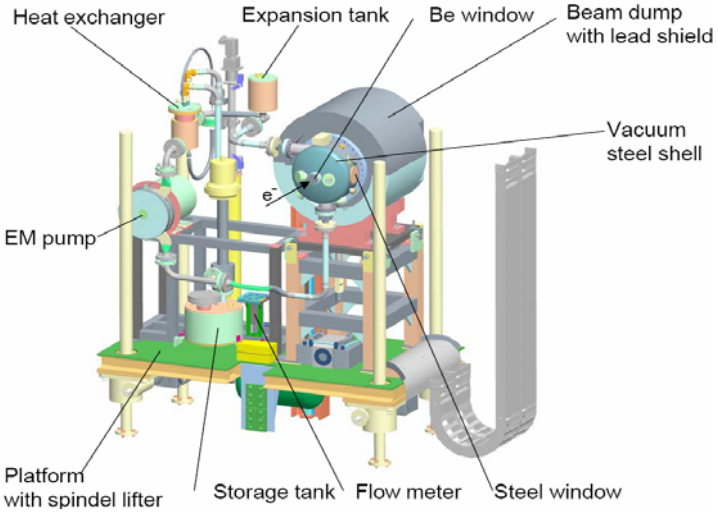

Fig. 2: 3D sketch of the pulsed neutron radiator

The final design of the photo-neutron source essentially consisting of the liquid lead loop including the e- target section, the beam dump, and the vacuum chamber housing the radiator is shown in Fig. 2. Due to the necessity for a movable radiator the electron beam has to be guided through two beryllium windows confining the high vacuum of the electron beam and the vacuum around the radiator. The latter Be window can also be seen in Fig. 2. The liquid Pb is circulated by an electromagnetic (EM) pump in a circuit made mainly from low activation stainless steel. The radiator section (where the e- beam hits the Pb) is made from Mo (see Fig. 3). The whole circuit is equipped with electric heaters to reach the operating point at 400 °C. The heat exchanger cools down the Pb from ≈ 470 °C to 400 °C.

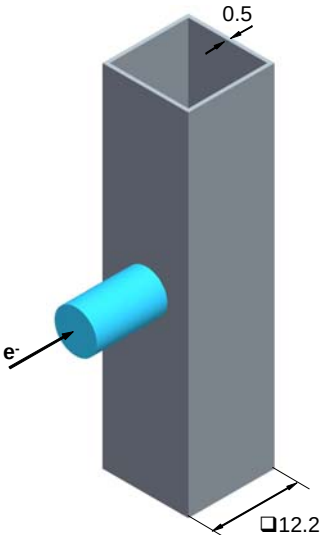

Fig. 3: Sketch of the Mo channel of the radiator with the electron beam of ELBE indicated

The electrons that are not stopped in the Pb radiator and the bremsstrahlung both concentrated in a forward peaked cone are dumped in an aluminum cylinder behind the target. About 50 % of the initial power of the electron beam will be deposited in the dump (e.g., for $E_{e^-} = 40$ MeV and $I_{e^-} = 1$ mA the initial power is 40 kW with 20 kW deposited). The dump is directly cooled by water and housed in a Pb shell in order to minimize heat radiation from the dump to other components of the photo-neutron source and to comply with radiation protection prescriptions.

The photo-neutrons that are radiated isotropically from the target are decoupled to the collimator under an angle of about 90° relative to the electron beam line through a thin steel window of the vacuum chamber to lower the background of photons, electrons and scattered neutrons at the measuring position. The whole construction follows the basic principle to have as little material in the range of view of the collimator as possible. For the same reason, the wall thickness of the vacuum chamber is also reduced at the side opposite to the neutron window to avoid backscattering of neutrons to the collimator that would decrease the achievable time resolution.

3.1. Radiator

The material selection of the radiator has to satisfy neutronic and thermo-mechanical criteria. Soon it became clear that liquid lead is the best material. So, it was the main task of the neu-

tronic and thermo-mechanic calculations to find the right wall material and best target size.

A material depth and width in the order of two radiation lengths (11.2 mm) was found to be optimum considering the finite size of the electron beam spot on the radiator. Further increasing the cross section of the lead radiator does not result in significant gain in neutron intensity but leads to broader neutron pulses due to multiple scattering in the radiator. Anticipating the result of the thermo-mechanical design, the lead flows through a Mo channel with a wall thickness of 0.5 mm (Fig. 3). For this target configuration, the MCNP [7] calculations predict a maximum source strength of $2.7 \cdot 10^{13}$ n/s and a maximum average neutron flux of about $1.5 \cdot 10^{7}$ n/(cm^2 s) at the measuring position 3.9 m away from the radiator for $E_{e^-} = 40$ MeV electrons and an electron current of $I_{e^-} = 1$ mA (Table 2). It can also be concluded from Table 2 that the source strength as well as the neutron flux at the measuring position sensitively depend on the electron energy.

Table 2: Neutron source strength and neutron flux at the measuring position after a flight path of L = 3.9 m with an electron current of $I_{e^-} = 1$ mA.

Electron energy in MeV	Neutron source strength at the radiator in n/s	Neutron flux at the measuring position in n/(cm^2 s)
20	$7.9 \cdot 10^{12}$	$4.3 \cdot 10^{6}$
30	$1.9 \cdot 10^{13}$	$1.0 \cdot 10^{7}$
40	$2.7 \cdot 10^{13}$	$1.5 \cdot 10^{7}$

The MCNP calculation yields a width of the neutron pulse at the radiator of 280 ps (FWHM) for an electron beam with an incident energy of $E_{e^-} = 40$ MeV and a diameter of $d_b = 3$ mm. With the assumed absolute detector time resolution of 600 ps, the energy resolution at the measuring position is better than 1 % for neutron energies $E_n < 4.5$ MeV. The particle energy spectra at the radiator show that the usable neutron energies range up to 10 MeV.

Different materials were considered as candidates for the wall of the radiator channel [4]. Mo turned out to be a feasible wall material with very high fracture strain even at room temperature (RT) and high thermal conductivity. The material tests proved its chemical resistance to the liquid lead. Due to the static pressure in the lead circuit a wall thickness of 0.5 mm (see Fig. 3) had to be chosen.

The local heat generation rates were calculated for all components of the photo-neutron source using the Monte-Carlo Code FLUKA [8, 9]. Assuming $E_{e^-} = 50$ MeV and beam diameters of $d_b = 3$ mm and 8 mm at the surface of the Mo channel, the maximum heat generation rate in the liquid lead is approximately 249 kW/cm³ and 46 kW/cm³ respectively. The numerical flow and heat transfer simulations for the radiator were performed using the multi-purpose finite elements code FIDAP [10]. The calculations of the temperature distribution in the radiator section were performed assuming mean flow velocities of $\langle v_{Pb} \rangle = 1$ m/s, 2 m/s, and 5 m/s and a lead temperature of 400 °C at the inlet to the neutron radiator channel. The maximum temperatures change only slightly for different beam energies. In contrast to that, the beam diameter has a significant influence to the maximum temperatures. For the beam diameter of $d_b = 8$ mm, all considered lead velocities yield temperatures uncritical with respect to the mechanical strength. For the beam diameter of $d_b = 3$ mm this holds only for the velocity of $\langle v_{Pb} \rangle = 5$ m/s. In all calculations, the maximum temperatures in the wall are by far lower than the melting temperature of Mo and the maximum temperatures in the liquid Pb are lower than the boiling temperature of Pb. Notwithstanding that, the cooling loop for the lead was designed for a mean velocity of at least $\langle v_{Pb} \rangle = 2$ m/s in the radiator channel to have a sufficient safety margin.

The mechanical analyses of the radiator channel were done with the finite element code ANSYS® [11]. Deflections, stresses, and strains were calculated. The construction of the Pb loop has to ensure that no significant thermal stresses occur. As a consequence of the strong temperature gradients a local plastification of the channel wall is unavoidable. In this context, the high ductility and the relatively low thermal expansion coefficient are significant advantages of Mo. The results show that from the mechanical point of view there is no risk of destruction of the radiator channel. Mo fulfills the thermal and mechanical requirements of the radiator channel. Fig. 4 shows the results of the two calculations.

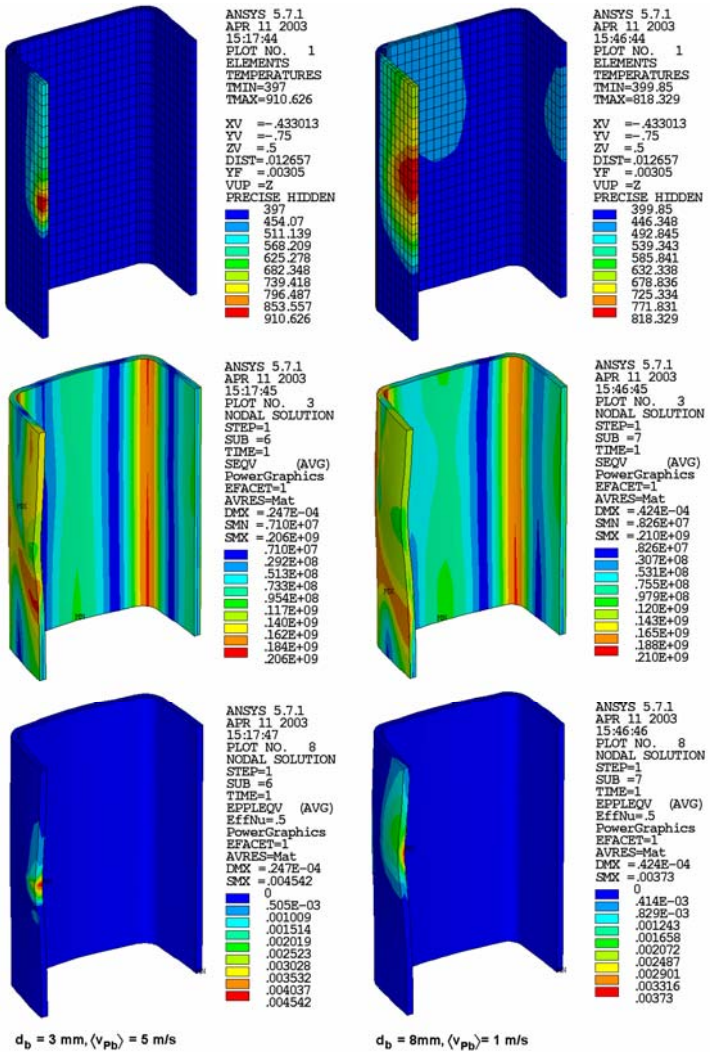

Fig. 4: Mechanical analysis results; top: temperature load T_{Mo} [°C]; middle: equivalent stress [Pa]; bottom: plastic equivalent strain; left side: d_b = 3 mm and $\langle v_{Pb} \rangle$ = 5 m/s; right side: d_b = 8 mm and $\langle v_{Pb} \rangle$ = 1 m/s

3.2. Beam dump

Pure Al was selected as dump material since it is a low activation material and because of its good thermal conductivity. Additionally, the cylindrical Al core has a cone-shaped notch (diameter and depth 100 mm) in the centre of the front side. The major part of the scattered electron beam hits the beam dump at this cone surface. A stainless steel tube coil is placed in the Al body. It guides the cooling water flow to prevent corrosion effects due to direct contact of the Al with the cooling water. To ensure that the deposited heat can safely be removed from the beam dump, a thermal analysis was performed [12]. The local heat generation densities were taken from the FLUKA calculations, which predict a maximum volumetric heat source of about $P_{heat,\,max}$ = 0.05 kW/cm³ that is obviously much lower than in the liquid lead target.

For E_{e-} = 50 MeV and d_b = 8 mm, corresponding to a total heat input of 24 kW into the dump, the maximum temperature in the Al body is ≈ 197 °C, which offers a sufficient distance from the melting point ($T_{Al,melt}$ = 660 °C). The maximum temperature in the Pb shielding is ≈ 101°C, which is also sufficiently far from the melting point ($T_{Pb,melt}$ = 327 °C). If the electron beam would not fully hit the radiator due to misalignment (leading to a roughly doubled deposited energy) the dump would partly melt. Therefore, it is mandatory to monitor the beam position or the Al temperatures and to immediately switch off the beam in case of misalignment.

4. Radiation background and neutron pulse structure at the measuring position

MCNP calculations of the background and flux at the measuring position 3.9 m away from the radiator were carried out taking into account the construction of the whole radiator set-up and a simplified neutron collimator. For reduction of background and increase of flux at the measuring position two concepts were pursued, 1st: remove material, especially near the radiator, out of sight of the collimator, 2nd: reduce the background of thermal neutrons from the collimator by boric polyethylene as cladding material of the collimator. Almost 92 % of the neutrons stem from the lead in the radiator, ≈8 % are scattered or generated in the Mo channel. A small fraction (< 0.1 %) is scattered in the steel housing accommodating the radiator. This background is due to materials close to the radiator which are in sight of the collimator.

The calculations also showed that a flight path of about L = 3.9 m allows separating neutrons from bremsstrahlung and electrons simply by their time of arrival at the measuring position. Neglecting all constructional components except the Pb-Mo radiator, MCNP yields a total average neutron flux of about $1.5 \cdot 10^7$ n/(cm^2 s) at the measuring position presuming an electron energy of E_{e^-} = 40 MeV and an electron current of I_{e^-} = 1 mA (Table 2). In Fig. 5, the neutron flux at the measuring position due to a single electron pulse is shown as function of time of arrival for E_{e^-} = 20, 30 and 40 MeV and for an electron bunch charge of Q_{e^-} = 2 nC, which will only be possible with the new superconducting SRF gun (Table 1). In the MCNP calculation, the e-pulse is δ-shaped and hits the radiator at t = 0 ns. Fig. 5 shows that the neutron flux increases with increasing neutron energy. The neutron pulse at the measuring position reaches the maximum flux at t ≈ 170 ns. This corresponds to a neutron energy of about 2.7 MeV. The neutron flux is too small for cross section measurements before t = 90 ns. Hence, there is a maximum usable neutron energy of about 10 MeV, which corresponds to a time-of-flight of 89.2 ns. The electron beam repetition rate determines the lowest usable neutron energy as faster neutrons from the next pulse start to overlap at the target position with slower neutrons from the preceding pulse. At t = 13 ns the prompt photons reach the measuring position. Using a repetition rate of f_{e^-} = 0.5 MHz the next bunch of photons arrives at t = 1/(0.5 MHz) + 13 ns = 2013 ns. This determines the lowest usable neutron energy at E_n = 19.6 keV. Slower neutrons will be absorbed or scattered out of the neutron beam by a removable absorber in the beam line. Using the SRF gun with the repetition rate of f_{e^-} = 0.5 MHz the measurable neutron energy range is roughly between E_n ≈ 50 keV and 10 MeV.

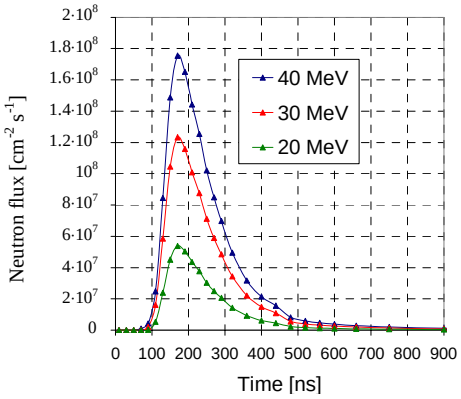

Fig. 5: Time dependent neutron flux at the measuring position due to a δ-shaped electron pulse, (Q_{e^-} = 2 nC, L = 3.9 m, E_{e^-} = 20, 30, 40 MeV, d_b = 3 mm)

5. Conclusion and outlook

The ELBE radiation source offers suitable parameters for neutron time-of-flight experiments for energy dispersive studies of the interaction of fast neutrons with matter. The calculations predict a maximum source strength of $2.7 \cdot 10^{13}$ n/s and a maximum average neutron flux at the measuring position of about $1.5 \cdot 10^7$ n/(cm^2 s). The neutron pulse at the measuring position reaches the maximum flux at a neutron energy of about E_n = 2.7 MeV. Using the new SRF photo electron injector with the repetition rate of f_{e^-} = 0.5 MHz the measurable neutron energy range is between E_n = 50 keV and 10 MeV. The expected energy resolution at the measuring

position is better than 1 % for energies up to 5 MeV. The estimated background at the measuring position is low. Further particle transport calculations are just being carried out to optimize the design of the collimator. Moreover, detectors are being developed for the detection of neutrons, photons and light charged particles and are tested at the ELBE bremsstrahl.

Concerning the thermal mechanical analyses, liquid lead proved to be a feasible material for the neutron radiator. This concept enables the save removal of the extremely high power densities of up to P_{heat} = 50 kW/cm³ which are generated by the interaction of the electron beam with the radiator material. It could be shown that the temperatures in the liquid lead and in the channel wall are low enough for save operation. Molybdenum turned out to be the most suited material for the radiator channel due to its high melting point, high ductility, good heat conductivity, and low thermal expansion. The plastic strain induced by the thermal load does not endanger the mechanical integrity of the channel. The energy deposited in the beam dump caused by electrons not stopped in the radiator and by secondary radiation can be safely removed by water cooling of the aluminum body.

The commissioning of the pulsed photo-neutron source and first neutron measurements are scheduled for 2007.

References

[1] M. Cometto, P. Wydler and R. Chawla (2004), A comparative physics study of alternative long-term strategies for closure of the nuclear fuel cycle, Annals of Nuclear Energy, 31, 413-429.

[2] J. Knebel et al. (2006), European Research Programme for the transmutation of high level nuclear waste in an accelerator driven system, Proceedings of the Conference on EU Research and Training in Reactor Systems (FISA 2006) (p. 322), Luxembourg

[3] G. Aliberti et al. (2006), Nuclear data sensitivity, uncertainty and target accuracy assessment for future nuclear systems, Annals of Nuclear Energy, 33, 700-733.

[4] J. Teichert et al. (2005), Progress of the Rossendorf SRF gun project, Proceedings of the 27th International Free Electron Laser Conference, Stanford, California, USA

[5] E. Altstadt et al. (2005), Energiedispersive Untersuchung der Wechselwirkung schneller Neutronen mit Materie, Rossendorf, Report FZR-426

[6] E. Altstadt et al. (2007), A photo-neutron source for time-of-flight measurements at the radiation source ELBE, Annals of Nuclear Energy, 34, 36-50

[7] J. F. Briesmeister (1993), MCNP a general MONTE CARLO N-Particle Transport Code, Version 4A, LA 12625 M

[8] A. Fasso et al. (2003), The physics models of FLUKA: status and recent developments, Conference on Computing in High Energy and Nuclear Physics 2003 (CHEP2003), eConf C0303241 (2003), arXiv:hep-ph/0306267, La Jolla, CA, USA

[9] A. Fasso, A. Ferrari, J. Ranft, P. R. Sala (2005), FLUKA: a multi-particle transport code, CERN, INFN/TC_05/11, SLAC-R-773.

[10] Fluent, Inc. (1998), FIDAP 8 Theory Manual, Lebanon, NH, USA

[11] ANSYS (1999), User's Manual for Rev. 5.6, Swansons Analysis Systems, Inc.

[12] H. Bergander (2003), FEM-Thermalberechnung des Beam Dump eines Neutronenproduktionstargets, Dresden, Germany, Technical Report HTS GmbH

Acknowledgement

This work was supported by Deutsche Forschungsgemeinschaft under contract FR 575/5 and GR 1674/2.